

Conductivity of anisotropic inhomogeneous superconductors above critical temperature.

S.S. Seidov,¹ K.K. Kesharpu,¹ P.I. Karpov,^{1,*} and P.D. Grigoriev^{2,1,3,†}

¹*National University of Science and Technology MISiS, Moscow, Russia*

²*L.D. Landau Institute for Theoretical Physics, 142432, Chernogolovka, Russia*

³*P.N. Lebedev Physical Institute, RAS, 119991, Moscow, Russia*

(Dated: October 2, 2018)

We propose a model and derive analytical expressions for conductivity in heterogeneous fully anisotropic conductors with ellipsoid superconducting inclusions. This model and calculations are useful to analyze the observed temperature dependence of conductivity anisotropy in various anisotropic superconductors, where superconductivity onset happens inhomogeneously in the form of isolated superconducting islands. The results are applied to explain the experimental data on resistivity above the transition temperature T_c in the high-temperature superconductor $\text{YBa}_2\text{Cu}_3\text{O}_8$ and in the organic superconductor $\beta\text{-(BEDT-TTF)}_2\text{I}_3$. The comparison of resistivity data and diamagnetic response in $\beta\text{-(BEDT-TTF)}_2\text{I}_3$ allows us to estimate the size of superconducting inclusions as $d \sim 1\mu\text{m}$.

PACS numbers: 74.81.-g, 74.25.fc, 74.72.-h, 74.70.-b, 74.70.Xa, 74.70.Kn, 74.62.-c

I. INTRODUCTION

The appearance of superconductivity with a temperature decrease in many compounds occurs nonuniformly along the sample. Such an inhomogeneous superconductivity onset is typical for the majority high-temperature superconductors (SC), e.g., copper-oxide and iron-based,¹⁻⁴ and it has been directly observed in numerous scanning tunneling microscopy (STM) experiments on various compounds⁴⁻¹⁰. The two main reasons for this inhomogeneity are the non-stoichiometry, coming from doping, and the interplay between different types of electronic ordering, often leading to phase separation. The diamagnetic response and the decrease of resistivity far above the superconducting transition temperature T_c are the typical precursors of inhomogeneous superconductivity,¹¹⁻²³ which cannot be explained^{14,20} by the standard theory²⁴ of superconducting fluctuations. Using scanning SQUID microscopy, such diamagnetic response was even shown to be highly inhomogeneous and extending far above T_c .^{13,15} Thus, in 500-nm-thick $\text{La}_{2-x}\text{Sr}_x\text{CuO}_4$ films with $T_c = 18\text{K}$ the diamagnetic domains of the size $\sim 5 - 200\mu\text{m}$ were observed up to a temperature $80\text{K} \gg T_c$ and attributed to isolated superconducting islands as precursors of superconductivity onset.¹³ With lowering temperature these superconducting islands become larger and finally cover most of the area at $T \approx T_c$.¹³ Similar diamagnetic domains of the size $\sim 100\mu\text{m}$ above T_c were also observed in $\text{YBa}_2\text{Cu}_3\text{O}_{7-y}$ films.¹⁵

The materials, where superconductivity onset shows such spatial inhomogeneity, are usually characterized by layered crystal structure and strong anisotropy of electronic properties. The resistivity drop above T_c in these compounds is often much stronger along the least conducting axis¹⁷⁻²³, which again contradicts²⁰ (see Appendix A for details) the theory^{24,25} of superconduct-

ing fluctuations in homogeneous superconductors. This anisotropic effect of incipient superconductivity was recently explained^{19,20} using a classical effective-medium model²⁶ for strongly anisotropic heterogeneous quasi-2D metal with spheroidal superconducting inclusions, which is a generalization of the well-known Maxwell's approximation²⁶ for the case of an anisotropic media with non-spherical inclusions. This simple model predicts^{19,20} that if superconductivity in anisotropic conductors appears in the form of isolated superconducting islands, it reduces electric resistivity anisotropically with the maximal effect along the least conducting axis.

The qualitative idea behind this model^{19,20} is simple. In a strongly anisotropic conductor with interlayer conductivity σ_{zz} much less than intralayer conductivity $\sigma_{xx} \sim \sigma_{yy}$, the first, standard way of interlayer current perpendicular to the conducting layers is small by the parameter $\eta \equiv \sigma_{zz}/\sigma_{xx} \ll 1$. However, there is a second way via superconducting islands. Since these islands are rare, the major part of the current path goes in the normal phase. But instead of going along the weakly-conducting z -axis in the non-superconducting phase, this second current path between the superconducting islands goes along the highly conducting layers, until it comes to another superconducting island, which allows the next lift in the interlayer direction. Then there is no local current density along the z axis in the non-superconducting phase, and the interlayer conductivity contribution from this channel does not acquire the small anisotropy factor $\sigma_{zz}/\sigma_{xx} \ll 1$. Instead, it acquires another small factor – the volume fraction ϕ of the superconducting phase. If the ratio $\phi/\eta \gtrsim 1$, the second way makes the main contribution to the interlayer conductivity.

In Refs. [19,20], analytical formulas for conductivity in such heterogeneous superconductor were obtained. These formulas provide a good quantitative agreement with experimental data on resistivity in FeSe and allow extracting the temperature dependence of the vol-

ume fraction ϕ of the superconducting phase in this compound.^{19,20} If experimental data on the temperature dependence of diamagnetic response are available in addition to transport measurements, their comparison also suggests the approximate shape of superconducting inclusions.²⁰ However, the obtained expressions^{19,20} for conductivity in such a heterogeneous superconductor are applicable only for the case when electronic properties in the conducting $a - b$ plane are isotropic. In FeSe it works well because in spite of the nematic transition at $T \approx 90\text{K}$,^{2,3} breaking the $a - b$ isotropy, the real crystals of FeSe consist of a large number of nanoscale monocrystals oriented differently along the a or b axis, which restores the $a - b$ isotropy on average. This $a - b$ isotropy in FeSe can be easily broken by applying a uniaxial pressure.

The limitation to only the isotropic quasi-2D case does not allow application of the expressions for conductivity of Refs.[19,20] to a large number of superconducting compounds with fully anisotropic electronic properties, where resistivity along all three main axes differs. Among such fully anisotropic compounds are most organic metals,^{27,28} where there are extensive experimental data on resistivity anisotropy above the superconducting transition temperature T_c . These data often show a much stronger effect of incipient superconductivity on interlayer resistivity above T_c ,²¹⁻²³ which is qualitatively consistent with the model^{19,20} of heterogeneous superconductivity onset. In many organic superconductors there are quasi-1D Fermi-surface parts, and superconductivity competes with a charge- or spin-density wave, leading to their phase coexistence and possible spatial separation in some pressure interval, as e.g. in $(\text{TMTSF})_2\text{PF}_6$,²² $(\text{TMTSF})_2\text{ClO}_4$,²³ or $\alpha\text{-(BEDT-TTF)}_2\text{KHg(SCN)}_4$.²⁹ The type of such phase coexistence and the corresponding microscopic structure of superconductivity in these compounds is still debated,^{22,23,29-34} but this density-wave state can be suppressed by pressure of several kbar.^{27,28} Some organic superconductors, e.g. $\beta\text{-(BEDT-TTF)}_2\text{I}_3$,²¹ $\kappa\text{-(BEDT-TTF)}_2\text{Cu[N(CN)}_2\text{]Br}$,³⁵ $\kappa\text{-(BEDT-TTF)}_2\text{Cu(NCS)}_2$,³⁶ have only quasi-2D Fermi surfaces, which are anisotropic in the conducting plane but do not have a nesting property, and hence they are not subject to Peierls or density-wave instability even at ambient pressure. The temperature dependence of resistivity anisotropy, shown in Fig. 6 of Ref. [21], reveals a stronger decrease of interlayer resistivity ρ_c as compared to ρ_a and ρ_b above the metal-superconductor transition, which may signify an inhomogeneous superconductivity onset according to the model of Refs. [19,20]. In many cuprate high- T_c superconductors, such as $\text{YBa}_2\text{Cu}_4\text{O}_8$, the chains between conducting layers break the $a - b$ isotropy. The $a - b$ isotropy in cuprates may also become broken due to the stripe electronic ordering, as proposed for $\text{La}_{2-x}\text{Sr}_x\text{CuO}_4$ ($x = 0.02 - 0.04$) and $\text{YBa}_2\text{Cu}_6\text{O}_y$ ($y = 6.35 - 7.0$).³⁷ In many iron-based high- T_c superconductors the $a - b$ isotropy is also often broken in the detwinned crystals.³⁸

In this paper we derive analytical expressions for conductivity in a fully anisotropic conductors with ellipsoid superconducting inclusions, thus removing the limitation of in-plane isotropy used in Refs. [19,20]. Then we apply our results to analyze the experimental data on the temperature dependence of resistivity along three main axes above T_c in the high- T_c superconductor $\text{YBa}_2\text{Cu}_4\text{O}_8$ and in the organic superconductor $\beta\text{-(BEDT-TTF)}_2\text{I}_3$.

The paper is organized as follows. In Sec. II we describe the mapping of the conductivity problem from the anisotropic to the isotropic case. In Sec. III we present our main analytical results for the anisotropic conductivity problem with the superconducting inclusions (some technical details are also described in Appendix B). In Sec. IV we apply the derived analytical results to the analysis of experimental data on $\text{YBa}_2\text{Cu}_4\text{O}_8$ and $\beta\text{-(BEDT-TTF)}_2\text{I}_3$. In Sec. V and VI we present a discussion and conclusions.

II. MAPPING OF CONDUCTIVITY PROBLEM IN ANISOTROPIC MEDIA TO ISOTROPIC

First, consider a homogeneous anisotropic conducting medium with conductivities $\sigma_{xx}^m, \sigma_{yy}^m, \sigma_{zz}^m$ along the principal axes. The electrostatic continuity equation for the medium can be written as

$$-\nabla \mathbf{j} = \sigma_{xx}^m \frac{\partial^2 V}{\partial x^2} + \sigma_{yy}^m \frac{\partial^2 V}{\partial y^2} + \sigma_{zz}^m \frac{\partial^2 V}{\partial z^2} = 0. \quad (1)$$

Here \mathbf{j} is the current density and V is the electrostatic potential. By the change of the coordinates

$$x = x', \quad y = \sqrt{\mu}y', \quad z = \sqrt{\eta}z', \quad (2)$$

where

$$\mu = \frac{\sigma_{yy}^m}{\sigma_{xx}^m}, \quad \eta = \frac{\sigma_{zz}^m}{\sigma_{xx}^m} \quad (3)$$

and by the simultaneous change of conductivity to $\sigma^m = \sigma_{xx}^m$ it transforms to the electrostatic continuity equation for isotropic media:

$$-\nabla \mathbf{j} = \sigma^m \left(\frac{\partial^2 V}{\partial x'^2} + \frac{\partial^2 V}{\partial y'^2} + \frac{\partial^2 V}{\partial z'^2} \right) = 0. \quad (4)$$

Hence, the initial problem of conductivity in anisotropic media with some boundary conditions can be mapped to the conductivity problem in isotropic media with new boundary conditions, obtained from the initial ones by the anisotropic dilatation given by Eq. (2).

Second, consider spherical inclusion particles with radii a_1 inside the media. Under the transformation (2), these spherical inclusions $x^2/a_1^2 + y^2/a_1^2 + z^2/a_1^2 = 1$ transform to ellipsoidal ones $x^2/a_1^2 + y^2/a_2^2 + z^2/a_3^2 = 1$ with semi-axes

$$a_1, a_2 = a_1/\sqrt{\mu}, a_3 = a_1/\sqrt{\eta}. \quad (5)$$

If x is the direction of highest conductivity of the medium and z is the direction of lowest conductivity (i.e. if $\sigma_{xx}^m > \sigma_{yy}^m > \sigma_{zz}^m$), then $\mu < \eta < 1$ and the ellipsoids become z -elongated (i.e. $a_3 > a_2 > a_1$). Note that generally μ and η can be temperature-dependent.

If initially the inclusions are not spherical but have an ellipsoidal shape with the principal semiaxes $a = a_1$, $b = \beta a_1$ and $c = \gamma a_1$, then after the mapping to the isotropic media these inclusions keep the ellipsoidal shape but change the principal semiaxes to

$$a_1, a_2 = a_1 \beta / \sqrt{\mu}, a_3 = a_1 \gamma / \sqrt{\eta}. \quad (6)$$

III. CONDUCTIVITY WITH ELLIPSOIDAL SUPERCONDUCTING INCLUSIONS

Using the mapping described in the previous section, the conductivity problem of an anisotropic conductive medium with some inclusion particles can be mapped to an effective isotropic media problem with the different shapes of the particles.

Here we consider a medium, e.g. a normal metal, with the isotropic conductivity σ_m , containing ellipsoidal islands with conductivity σ_{isl} and the volume fraction ϕ . The macroscopic conductivity of the sample $\sigma^* = \text{diag}(\sigma_{xx}^*, \sigma_{yy}^*, \sigma_{zz}^*)$ in the effective-medium Maxwell's approximation, applicable for $\phi \ll 1$, can be obtained from (see Eqs. (18.9) and (18.10) of Ref. [26])

$$(1 - \phi)(\sigma_i^* - \sigma^m) + \phi \frac{\sigma_i^* - \sigma^{isl}}{1 + A_i(\sigma^{isl} - \sigma^m)/\sigma^m} = 0, \quad (7)$$

where $i = 1, 2, 3$ corresponds to x, y, z axes, and coefficients A_i are given by (see Eq. (17.25) of Ref. [26]):

$$A_i = \frac{a_1 a_2 a_3}{2} \int_0^\infty \frac{dt}{(t + a_i^2) \sqrt{(t + a_1^2)(t + a_2^2)(t + a_3^2)}}. \quad (8)$$

The integrals can be evaluated analytically (see Appendix B). For superconducting islands $\sigma^{isl} \rightarrow \infty$, Eq. (7) simplifies to

$$(1 - \phi)(\sigma_i^* - \sigma^m) - \phi \frac{\sigma^m}{A_i} = 0. \quad (9)$$

Solving it for σ_i^* we obtain

$$\sigma_i^*(\phi) = \sigma^m \left(1 + \frac{\phi}{A_i(1 - \phi)} \right) \approx \sigma^m \left(1 + \frac{\phi}{A_i} \right). \quad (10)$$

One can also calculate the resistivity

$$\rho_i^*(\phi) = \frac{1}{\sigma_i^*(\phi)} = \frac{1}{\sigma^m} \frac{A_i(1 - \phi)}{\phi + A_i(1 - \phi)} \approx \frac{1}{\sigma^m} \frac{1}{1 + \phi/A_i}. \quad (11)$$

Transforming back from coordinates (x', y', z') of the isotropic media to the original coordinates (x, y, z) of the anisotropic one (see Eq. (2)), we obtain the final result

for resistivities along the three principal axes of heterogeneous anisotropic media with elliptic superconducting inclusions:

$$\rho_1(\phi) = \frac{1}{\sigma^m} \frac{A_1(1 - \phi)}{\phi + A_1(1 - \phi)}, \quad (12)$$

$$\rho_2(\phi) = \frac{1}{\mu \sigma^m} \frac{A_2(1 - \phi)}{\phi + A_2(1 - \phi)}, \quad (13)$$

$$\rho_3(\phi) = \frac{1}{\eta \sigma^m} \frac{A_3(1 - \phi)}{\phi + A_3(1 - \phi)}, \quad (14)$$

where A_i are given by Eqs. (B1)-(B3) for arbitrary ratios of ellipsoid semiaxes, or by Eqs. (B4)-(B6) for $a_3 \gg a_1, a_2$.

IV. COMPARISON WITH EXPERIMENTS

In this section we apply the developed model to the analysis of two superconducting compounds at $T > T_c$, namely, the high- T_c superconductor $\text{YBa}_2\text{Cu}_4\text{O}_8$ and the organic superconductor $\beta\text{-(BEDT-TTF)}_2\text{I}_3$.

A. High- T_c superconductor $\text{YBa}_2\text{Cu}_4\text{O}_8$

Here we analyze the high- T_c superconductor $\text{YBa}_2\text{Cu}_4\text{O}_8$ at $T > T_c$. In order to do this, we use the experimental data for the temperature dependence of resistivities $\rho_i(T)$ along three principal axes, extracted from Fig. 2 of Ref. [17] (in our notation, axes 1, 2, 3 with the descending resistivities correspond to axes b, a, c of Ref. [17]).

In order to calculate conductivity with the correction due to the superconducting inclusions we, first, need to know the temperature dependencies of conductivity in the non-superconducting (metallic) phase above T_c along the principal axes. These can be extracted from the experimental data in different ways. For example, if superconductivity can be suppressed by magnetic field, then conductivity in the high magnetic field is approximately the same as without field in the metallic phase. If such data are available, conductivity in the metallic phase above T_c can be extracted as an extrapolation from the high temperatures, where the effect of superconductivity is absent or negligible. In YBCO the available magnetic fields are not sufficient to suppress superconductivity, and we use extrapolation from higher temperatures.

Assuming that at high temperatures the volume fraction of superconducting inclusions ϕ goes to zero sufficiently fast, becoming negligible at $T > 250\text{K}$, we extract the resistivity of the medium from the high-temperature asymptotic behavior of $\rho_i(T)$: $\rho_i^m(T) \approx \rho_i(T)$ (here $\rho_i^m = 1/\sigma_i^m$). Along the z and y axes the resistivity is approximately linear at high T , and we extract $\rho_{yy}^m = (43.5 +$

$0.772\text{K}^{-1}T)\mu\Omega\text{cm}$, $\rho_{zz}^m = (6950 + 3.75\text{K}^{-1}T)\mu\Omega\text{cm}$. For the x -axis the total conductivity is approximately a sum of contributions from conducting planes and chains. The chain resistivity is not linear but rather a quadratic function of T .¹⁷ Hence, according to Ref. [17], we use the chain resistivity obtained from $1/\rho_{\text{chain}} = 1/\rho_{xx}^m - 1/\rho_{yy}^m$, with $\rho_{\text{chain}} = (0.5 + 0.00147\text{K}^{-2}T^2)\mu\Omega\text{cm}$. This gives $\rho_{xx}^m = \rho_{\text{chain}}\rho_{yy}^m/(\rho_{\text{chain}} + \rho_{yy}^m)$ and $\sigma^m = 1/\rho_{xx}^m$. Using Eq. (3), we obtain $\mu(T)$ and $\eta(T)$.

Solving equation (14) for ϕ we get

$$\phi(T) = \frac{1 - \eta\rho_3\sigma^m}{1 + \eta\rho_3\sigma^m(A_3^{-1} - 1)}. \quad (15)$$

Equations (12) and (13) can also be used for the same purpose of extracting $\phi(T)$, but $\rho_3(T)$ has the most pronounced drop with decreasing T (compared to the linear extrapolation from high to low temperatures), so it should give the most accurate results. The least-conductive z -direction has the smallest coefficient among A_i (see Eqs. (B7)-(B9)). Hence, according to Eq. (10), σ_{zz} is the most sensitive to the concentration of inclusions ϕ , unless the shape of superconducting inclusions is too compressed along the z -axis. Conductivity σ_{xx} along the highest conductive direction is expected to be the least sensitive to the variation of ϕ .

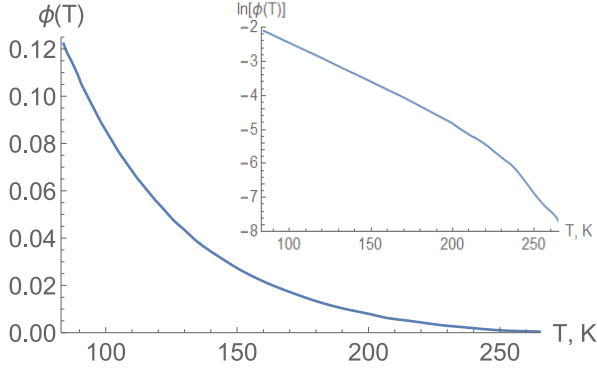


FIG. 1: Temperature dependence $\phi(T)$ of the volume fraction of superconducting inclusions extracted from formula (15) and the experimental data from Ref. [17] for $\text{YBa}_2\text{Cu}_4\text{O}_8$.

Assuming that the spatial extensions of the superconducting inclusions are proportional to the coherence lengths $\xi_i \sim v_i^F$ along the corresponding axes, we take the anisotropy parameters $\beta = v_y^F/v_x^F = 1$, because superconductivity comes from the conducting planes (not chains) where the electron dispersion is isotropic, and $\gamma \approx v_z^F/v_x^F \approx \sqrt{\sigma_{zz}/\sigma_{xx}} \approx 0.15$. This aspect ratio γ is very close to the aspect ratio $\gamma_o \approx 0.14$ giving the best fit of the resistivity curves within our model.

Figure 1 shows the temperature dependence $\phi(T)$, derived from Eq. (15) for the inclusions anisotropy parameters $\beta = 1$ and $\gamma = 0.15$. As expected, $\phi(T)$ decreases with the increase of temperature and becomes negligibly small (or zero) only at $T \gtrsim 250\text{K}$, which is much higher than the transition temperature $T_c = 78\text{K}$. As one can see

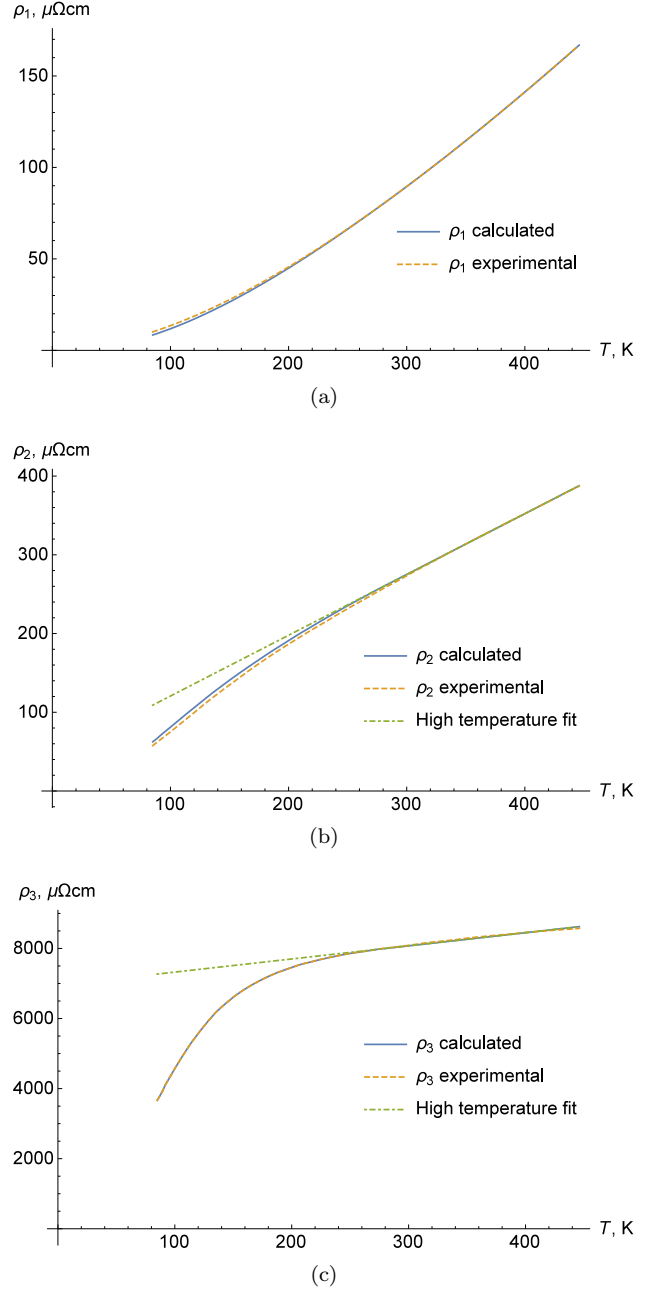


FIG. 2: Comparison between the proposed theory and the experimental data from Ref. [17] on the temperature dependence of resistivity in $\text{YBa}_2\text{Cu}_4\text{O}_8$ along three main axes, $\rho_i(T)$ for $i = 1, 2, 3$. In Fig. (a) the high-temperature fit coincides with experimental data and is not shown.

from the inset in Fig. 1, where $\phi(T)$ is plotted in the logarithmic scale, the dependence $\phi(T)$ is nearly exponential in the temperature range $80\text{K} < T < 200\text{K}$. This exponential decrease of $\phi(T)$ with increasing T is natural for the model of isolated superconducting inclusions coming from disorder or electronic phase separation, but it contradicts the prediction from the theory of superconducting fluctuations in homogeneous superconductors^{24,25}.

From $\phi(T)$ we derive $\rho_i(T)$ using formulas (12)-(14)

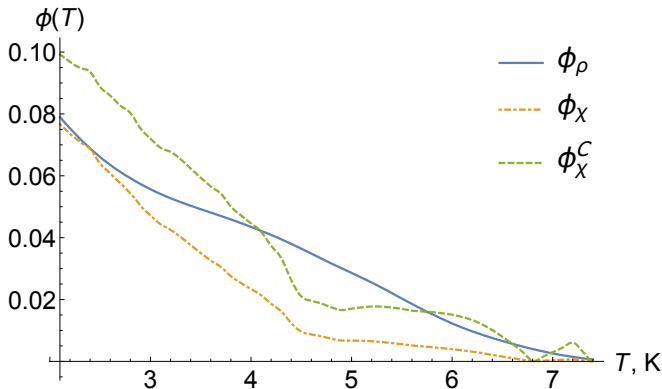


FIG. 3: Comparison of the temperature dependence of SC volume fraction ϕ in β -(BEDT-TTF) $_2$ I $_3$ calculated from the resistivity data²¹ (ϕ_ρ , solid blue curve, Eq. (15)), and from the magnetic susceptibility data⁴² using Eq. (16): with temperature-independent constant $C = 2600$ (ϕ_χ , orange dot-dashed curve) and with temperature-dependent coefficient $C(T)$ given by Eq. (18) (ϕ_χ^C , green dashed curve).

and in Fig. 2 we compare the obtained dependencies with the experimental data of Ref. [17]. The calculated dependence $\rho_3(T)$ trivially coincides with the experimental one, since we extracted $\phi(T)$ from ρ_3 . Also, naturally we get a good agreement for $\rho_1(T)$, since resistivity in the highest conductivity x -direction depends only weakly on ϕ , as explained above. The most important role here is played by $\rho_2(T)$ -dependence: the difference between the high-temperature fit (green dot-dashed line) and our theoretical prediction (blue solid line) comes from isolated superconducting inclusions according to the proposed model, which fits very well with the experimental data (orange dashed line).

B. Organic superconductor β -(BEDT-TTF) $_2$ I $_3$

In this subsection, we apply our theoretical model to analyze the observed temperature dependence of conductivity anisotropy in a quasi-2D organic charge transfer salt β -(BEDT-TTF) $_2$ I $_3$ with superconducting transition temperature $T_c \approx 1.5$ K^{21,39,40}. This compound is convenient for the analysis because (i) both resistivity along all three main axes and susceptibility data are available for it, and (ii) it does not have several complicating features characteristic of high- T_c cuprate superconductors.

We have taken the resistivity data $\rho_i(T)$ along three principal axes, extracted from Figs. 2, 3, 4 of Ref. [21] (in our notation, axes 1, 2, 3 with the descending resistivities correspond to axes a, b, c of Ref. [21]). The data from the sample denoted by the open circles (o) were used⁴¹.

Unfortunately, we have not found experimental data on resistivity in this compound under very high magnetic field, which prevents SC island formation. Therefore, to find the temperature dependence of metallic conductivity, we extrapolated resistivity along the highest

conductivity x -axis, from high temperatures $T > 9$ K down to $T = 2 \div 9$ K as: $\rho_{xx}^m \equiv \rho_1^m = (1.429 + 0.084\text{K}^{-1}T + 0.006\text{K}^{-2}T^2)\rho_1(293\text{K}) \times 10^{-3}$ (where the value of $\rho_1(293\text{K}) \approx 54.15$ m Ω cm was extracted from Ref. [21]). In this extrapolation we keep both linear and quadratic terms, which may come from the electron-electron interaction at low temperature. The volume fraction $\phi(T)$ of SC islands is found from the resistivity ρ_3 along the lowest conductivity z -axis, using Eq. (15) for the SC inclusions of the ellipsoidal shape with the principal semiaxes ratios $a_2 = a_3 = 3a_1$ in the mapped space, or $\beta = b/a \approx 2$, $\gamma = c/a \approx 0.13$ in real coordinate space. The parameters β and γ were found by minimizing the difference between the theoretical prediction and the experimental data for resistivity along the x and y axes. The result for $\phi(T)$ is shown in Fig. 3 by solid blue curve.

In Fig. 4 we compare the experimental data on resistivity with the predictions of our model. The experimental and theoretical curves for $\rho_3(T)$ trivially coincide because we used $\rho_3(T)$ data to obtain $\phi(T)$ using Eq. (15). The calculated temperature dependence of two other resistivity components $\rho_1(T)$ and $\rho_2(T)$, given by solid blue curves in Fig. 4, agrees well with the experimental data (dashed orange curves). The values of resistivity used in Fig. 4(a) and 4(b) at $T = 293$ K along a -axis ($\rho_1^{293\text{K}} = 54.15$ m Ω cm) and along b -axis ($\rho_2^{293\text{K}} = 86.64$ m Ω cm) respectively are calculated from the experimental data given in Ref. [21]. The high-temperature fit without SC inclusions is given by the green dot-dashed curve.

We can compare, at least qualitatively, the temperature dependence of the SC volume fraction $\phi_\rho(T)$, calculated from the resistivity data, with SC volume fraction $\phi_\chi(T)$, calculated from the magnetic susceptibility data, taken from Fig. 1 of Ref. [42]. In this figure the magnetic susceptibility $\chi_{2.8}$ in a weak magnetic field of 2.8 kOe has a pronounced drop. This drop starts at $T^* \approx 8$ K and was ascribed to incipient superconductivity, because in higher magnetic field 8.0 kOe the observed diamagnetic susceptibility $\chi_{8.0}$ does not have such a drop.⁴² The standard theory of SC fluctuations²⁴ does not explain such a large difference between $T^* \approx 8$ K and the SC transition temperature $T_c \approx 1.5$ K. Hence, also taking into account the resistivity data²¹, we suppose that the observed diamagnetic response originates from the SC islands, which survive only at lower magnetic field. Assuming that the low magnetic field 2.8 kOe almost does not affect the SC inclusions, and in high magnetic field 8 kOe, on the contrary, the effect of SC islands is negligible, we find that ϕ_χ is proportional to the difference $\Delta\chi \equiv (\chi_{2.8} - \chi_8)$, divided by the susceptibility $\chi_{SC} = -1/4\pi$ of a perfect superconductor:

$$\phi_\chi = C\Delta\chi/\chi_{SC}, \quad (16)$$

In Fig. 3 we compare SC volume fraction $\phi_\rho(T)$ (blue solid curve) extracted from the resistivity data²¹ with $\phi_\chi(T)$ (orange dot-dashed curve), determined according

to Eq. (16) with the constant coefficient $C = 2.6 \times 10^3$, found assuming that around 1.8-2K the values of $\phi_\rho(T)$ and $\phi_\chi(T)$ on average become close to each other.

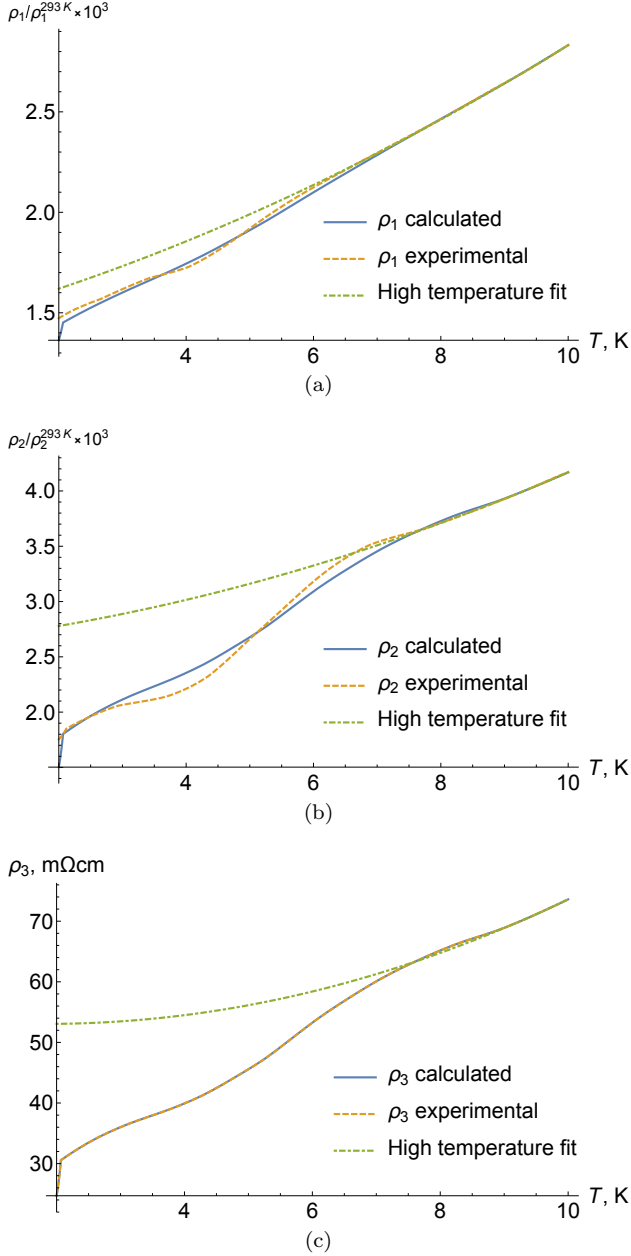


FIG. 4: Comparison between the proposed theory and the experimental data from Ref. [21] on the temperature dependence of resistivity in β -(BEDT-TTF) $_2$ I $_3$ along three main axes, $\rho_i(T)$ for $i = 1, 2, 3$. The high-temperature fit is the resistivity extrapolated from $T > 9$ K down to low temperatures and given by the second-order polynomials in T : $\rho_1^m(T) = (1.429 + 0.084\text{K}^{-1}T + 0.006\text{K}^{-2}T^2)\rho_1(293\text{K}) \times 10^{-3}$, $\rho_2^m(T) = (2.616 + 0.063\text{K}^{-1}T + 0.009\text{K}^{-2}T^2)\rho_2(293\text{K}) \times 10^{-3}$, and $\rho_3^m(T) = (47.821 + 0.025\text{K}^{-1}T + 0.255\text{K}^{-2}T^2)\text{m}\Omega\text{cm}$.

The coefficient C is not equal to unity mainly because of three effects: (i) the demagnetizing factor n of the SC ellipsoids, (ii) the finite penetration depth λ of a mag-

netic field into the SC granules, and (iii) the penetration of vortices if the applied magnetic field exceeds the lower critical field H_{c1} . Susceptibility of a macroscopic SC ellipsoid is given by $\chi_{\text{ellipsoid}} = (-1/[4\pi(1-n)])$,^{43,44}. The demagnetization factor n along the longest semi-axis of the ellipsoid with $b/a = 2$ and $c/a = 0.13$ is $n \approx 0.05$, as calculated from the Eq. (2.1) of Ref. [45].⁴⁶ Hence, the first effect only gives a factor $(1-n)^{-1} \approx 1.05 \sim 1$.

The second effect is more important if the penetration depth λ is comparable to or greater than the size $d = 2R$ of SC islands. Using the well-known expression for the diamagnetic susceptibility $\chi = -R^2/40\pi\lambda^2$ of a small spherical SC granule with radius $R \ll \lambda$ (see Eq. (8.22) of Ref. [25]), we can approximate the measured susceptibility decrease $\Delta\chi$ by

$$\Delta\chi \approx \frac{\chi_{\text{SC}}\phi_\chi R^2}{10\lambda^2(1-n)}. \quad (17)$$

The penetration depth λ depends on T and diverges at the critical temperature (see Eq. (2.3) of Ref.[25]): $\lambda(T) \approx \lambda(0)/\sqrt{1-(T/T_c)^4}$. Here, instead of the macroscopic zero-resistance value T_c we use the temperature T^* below which SC islands start to appear. This gives the temperature dependence of the constant C in Eq. (16) at $R \ll \lambda$:

$$C(T) \approx \frac{10\lambda^2(1-n)}{R^2} \approx \frac{10[\lambda(0)]^2(1-n)}{R^2[1-(T/T^*)^4]}. \quad (18)$$

For our estimate of the SC islands radius R we take $T^* \approx 8$ K because (i) there is a clear drop of interlayer resistivity at $T = 6 - 8$ K, suggesting the appearance of many SC islands below $T^* \approx 8$ K, and (ii) this T^* is close to the SC transition temperature $T_c \approx 7.5$ K of another group of crystals²¹ of the same compound but prepared in a different way. Moreover, this simplification only leads to a minor error in our estimate of the size of SC islands given below, because for this estimate we compared the SC volume fraction at $T = 2 - 4$ K (see Fig. 3), where the factor $[1 - (T/T^*)^4] \sim 1$ is not very sensitive to the precise value of T^* .

Eq. (18) explains why at high temperatures $T > 4$ K, when $\lambda(T)/\lambda(0) \gg 1$, there is a strong difference between ϕ_ρ and ϕ_χ calculated for a constant C . Therefore it is more physically motivated to use the SC volume fraction $\phi_\chi^C(T)$ which takes into account the temperature dependence of the coefficient $C(T)$. We extract $\phi_\chi^C(T)$ from the experimental data⁴² on susceptibility according to Eqs. (16) and (18) with $\lambda(0)/R = 16$; it agrees with $\phi_\rho(T)$ much better than for the temperature-independent coefficient C , as shown in Fig. 3. Thus we can estimate the typical size of the SC islands as $d = 2R \approx \lambda(0)/8$. The usual in-plane London penetration depth in organic metals is rather large, $\lambda(0) \gtrsim 1\mu\text{m}$, while the out-of-plane penetration depth is even ~ 30 times larger.⁴⁷ Using the in-plane London penetration depth $\lambda(0) \approx 6\mu\text{m}$ of the

compound α -(BEDT-TTF) $_2$ I $_3$ from the same family,⁴⁷ we obtain the typical size $d \approx 0.75\mu m \sim 1\mu m$ of SC inclusions in β -(BEDT-TTF) $_2$ I $_3$. This is much greater than the in-plane SC coherence length $\xi_{||} \approx 10 - 80nm$ ⁴⁸ in this compound. Thus the proximity effect and Josephson coupling give only small corrections to our formulas.

There is a third effect, influencing the diamagnetic response and the coefficient C in Eq. (18). Due to the penetration of magnetic vortices, if the applied magnetic field exceeds the lower critical field H_{c1} , then the diamagnetic signal of a bulk superconductor is much smaller than that of an ideal diamagnet. However, if the size of SC islands R is small, much smaller than SC penetration depth λ , the penetration of magnetic vortices to SC may be energetically unfavorable, so that no or very few vortices are in the small superconducting islands. The effective lower critical field in a thin cylinder of radius R at $\xi \ll R \ll \lambda$ was shown to increase $H_{c1} \propto (\lambda/R)^2$ (see Eq. (4) of Ref. [49]) and even exceed upper critical fields H_{c2} and H_{c3} at $R < 1.5\xi$ (see Fig. 1 of Ref. [49]). For $\lambda/R \approx 16$, as we estimated above, the magnetic field must exceed the bulk H_{c1} more than 300 times for the penetration of a single vortex becoming energetically favorable, which is, probably, not the case in the experiment in Ref. [42], although the applied magnetic field there is much larger than H_{c1} in a bulk superconductor. If the applied magnetic field in Ref. [42] exceeds this enlarged H_{c1} , a few vortices may penetrate the SC islands and reduce the diamagnetic response. Then our estimate of the SC island radius R from Eqs. (17) and (18) gives a lower bound for R . This is also helpful, because this lower bound is still larger than the SC coherence length, thus substantiating the applicability of our model.

V. DISCUSSION

In order to calculate the classical conductivity of heterogeneous media we have used the Maxwell's or Maxwell-Garnett approximation, generalized for anisotropic media. It is valid only in the limit of low volume fraction ϕ of the second phase, i.e. of superconducting inclusions in our case. In particular, it gives an incorrect percolation threshold $\phi = 1$. However, Maxwell's approximation has several important advantages: (i) it is exact in the limit $\phi \ll 1$; (ii) it coincides with the optimal Hashin-Shtrikman bounds,⁵⁰ i.e., it equals to the lower bound for the effective conductivity of media with superconducting inclusions for arbitrary ϕ ; (iii) it does not require the usually unknown information about the distribution function of superconducting islands and about their typical size d ; (iv) it gives a simple analytical result.

There are several other approaches to this classical conductivity problem that have their own advantages and drawbacks.^{26,50} Among the most popular analytic approaches, we have the self-consistent effective-medium approximation, the cluster expansions and the contrast expansions, giving various bounds for the effective con-

ductivity tensor. The self-consistent effective-medium approach is the simplest one after the Maxwell's approximation. It gives nontrivial percolation thresholds in 2D and 3D cases, which are close to the numerical results for the isotropic case. However, for anisotropic systems these percolation thresholds differ for different directions, which is incorrect in a general case. The self-consistent approximation does not have a strict substantiation even in the low- ϕ limit, but it was shown to describe correctly some fractal inhomogeneous structures, which are similar on different length scales.^{26,50} Thus, it is not clear if the self-consistent or Maxwell's approximation gives better accuracy for our strongly anisotropic case.

The cluster expansions coincide with Maxwell's approximation for the dilute dispersions of superconducting islands or in the first order in ϕ and give better accuracy in the higher orders. However, this approach requires the distribution and correlation functions of superconducting inclusions, which are unknown. In addition, the cluster expansions do not usually give simple analytical formulas. The contrast expansions work well when the conductivities of two phases do not differ much, which is not applicable to our case where the conductivity ratio is infinite. In addition, the contrast expansions also require the knowledge of the correlation function and do not give simple analytical results. The various numerical methods of calculating the effective conductivity of such a heterogeneous classical system⁵⁰ give much more accurate results but are not convenient for the physical analysis. In addition, the accuracy of our classical model is limited, especially without knowledge of size the distribution and the correlation function of superconducting islands. Thus, among various methods, the applied Maxwell-Garnett approximation seems to be reasonable for our qualitative study.

The applied classical model does not take into account several quantum superconducting features: the Andreev reflection, the proximity effect, and the Josephson coupling between superconducting islands.²⁵ All these three effects increase the electric conductivity in such a heterogeneous medium

The Andreev reflection increases an electric current through the normal-superconductor (N-S) interface. The increase depends on the strength of the potential barrier on this interface (see Sec. 11.5.1 of Ref. [25]), but it does not exceed the factor of 2. Since in our case the superconducting islands are made of the same material as the metallic matrix, the potential barrier at their interface is not large, and the Andreev reflection may almost double the current through a flat N-S interface. For an ellipsoidal or arbitrary shape of SC granules this increase factor is less than 2 and closer to unity; it should be taken into account in a rigorous quantitative theory, but is beyond our study.

The proximity effect creates a non-zero superconducting condensate in the surrounding shell of the thickness $\sim \xi$, around each of the superconducting islands. Since $\xi \propto v_F$ has the same anisotropy as electron velocity v_F ,

in layered compounds this shell is thicker along the conducting layers and thinner along the interlayer z direction. When the typical size d and distance l between SC islands are greater than ξ , the proximity effect is qualitatively equivalent to the effective increase of the SC island size by a length $\sim \xi$. Then it increases the calculated correction $\Delta\sigma_i$ to conductivity along the axis i due to SC islands by a quantity $\sim (\xi_i/d_i)\Delta\sigma_i$. For small SC islands of the size $d \lesssim \xi$ the proximity-effect correction to $\Delta\sigma_i$ is not small and must be taken into account in a quantitative theory, because it increases the effective volume fraction ϕ of SC phase and changes the effective shape of SC islands, making them closer to an ellipsoid with the main axes $d_i^* \propto \xi_i$. For naturally inhomogeneous superconductors, when both SC and metallic regions consist of the same compound, the size of SC islands $d \gtrsim \xi$, and our analysis remains valid. For example, in β -(BEDT-TTF) $_2$ I $_3$ the typical size of SC inclusions $d \sim \lambda/8(0) \sim 1\mu\text{m} \gg \xi_{||} \sim 10 - 80\text{nm} \gg \xi_{\perp} \sim 1\text{nm}$, and the proximity effect gives only a small correction. However, even in the case $d_{||} \lesssim \xi_{||}$ the qualitative effect that the strongest relative increase of conductivity due to SC islands is along the least conducting axes of metallic matrix may persist if $d_{\perp} \gtrsim \xi_{\perp}$.

For the small inter-island distance $l \lesssim \xi$, the Josephson coupling between superconducting inclusions becomes important. It gives the phase coherence to the SC condensates on the neighboring islands and may even lead to superconductivity of the whole sample if this phase coherence is long-range. The conductivity of an array of SC granules in a dielectric medium has been extensively studied in various regimes and the corresponding superconductor-insulator phase diagram has been obtained theoretically and experimentally (see Ref. [51] for a review). Arrays of SC granules in a metallic matrix received less attention but have also been investigated in artificial⁵² and natural^{53–55} systems. The metal-superconductor transition in these systems occurs in two stages. First, with lowering temperature, at $T < T_c^*$, superconductivity appears in isolated granules, which reduces electric resistivity and gives a diamagnetic response. At lower temperature, the long-range coherence between isolated SC islands or clusters are established, and at the resistive transition temperature $T_c < T_c^*$ the whole sample becomes superconducting. For a random spatial and T_c^* distribution of SC islands, this leads to a continuous decrease of resistivity between T_c^* and T_c . Finite-temperature effects break this coherence when T becomes comparable to the Josephson coupling energy $E_J \equiv \hbar I_c/2e$, where I_c is the critical current of the Josephson junction,²⁵ which depends exponentially on the intergranular distance l : $I_c \propto \exp(-l/\xi)$. Near T_c^* of SC granules the critical current has a linear temperature dependence, $I_c \propto T_c^* - T$, and for $l > \xi$ it acquires additional exponential temperature damping. Hence, in our limit of low volume ratio $\phi \ll 1$ of the SC phase, where $l > \xi$, the Josephson coupling is most probably suppressed by temperature and can be neglected.

Thus, the applied model is quantitatively valid only in the macroscopic limit, when the size of superconducting islands d and the distance between them l are much larger than the coherence length ξ . In the limit of low fraction $\phi \ll 1$ of the SC phase, when the applied Maxwell's approximation is valid, $l \gg d$. Then our analysis is quantitatively valid at $\xi_i \ll d_i$ and gives correct qualitative predictions at $\xi_i \lesssim d_i$. The typical size d of SC islands can be measured for a particular compound using the STM^{4–10} or scanning SQUID microscopy^{13,15}. In all these experiments the typical SC domain size d was at least several times larger than the SC coherence length ξ . The smallest SC domain size $d \gtrsim 3\text{nm}$ was detected in $\text{Bi}_2\text{Sr}_2\text{CaCu}_2\text{O}_{8+\delta}$,⁵ where the in-plane coherence length $\xi_{ab} \approx 1.6\text{nm}$, thus the ratio $d/\xi \gtrsim 2$. In $\text{YBa}_2\text{Cu}_6\text{O}_y$ the observed diamagnetic domain size was much greater,¹⁵ $d \sim 1\mu\text{m} \gg \xi_{ab} \sim 2\text{nm}$. In NbN the observed SC domains have the size $d \approx 20 - 50\text{nm} \gg \xi \sim 6\text{nm}$.⁷ In β -(BEDT-TTF) $_2$ I $_3$, as we estimated above, the size of SC islands is also $d \sim 1\mu\text{m} \gg \xi$. Thus, typically $d/\xi \gg 1$, and our formulas are applicable. However, we did not find any experimental data on the domain size in $\text{YBa}_2\text{Cu}_4\text{O}_8$.

Using torque magnetization measurements, in $\text{La}_{2-x}\text{Sr}_x\text{CuO}_4$, $\text{Bi}_2\text{Sr}_{2-y}\text{La}_y\text{CuO}_6$, $\text{Bi}_2\text{Sr}_2\text{CaCu}_2\text{O}_{8+\delta}$ and $\text{YBa}_2\text{Cu}_6\text{O}_y$ the diamagnetic response as a precursor of superconductivity was shown to survive at temperatures much higher than the superconducting transition temperature T_c .¹¹ In particular, in $\text{La}_{2-x}\text{Sr}_x\text{CuO}_4$ and $\text{Bi}_2\text{Sr}_{2-y}\text{La}_y\text{CuO}_6$ the onset temperatures T_{onset}^M of this diamagnetic response exceed more than three times T_c in a wide doping intervals and nearly coincide with the onset temperatures T_{onset}^N of enhanced Nernst signal (see Fig. 11 of Ref. [11]), presumably corresponding to the vortex-liquid state. Even in the optimally doped $\text{YBa}_2\text{Cu}_6\text{O}_y$ with $T_c \approx 92\text{K}$ the diamagnetic response is observed up to $T_{onset}^M \approx 130\text{K}$.¹¹ According to Ref. [4], it should coincide with the onset temperature T^* of pseudogap, which for $\text{YBa}_2\text{Cu}_4\text{O}_8$ exceeds 200K. Hence, it is not very surprising that some traces of superconductivity appear in $\text{YBa}_2\text{Cu}_4\text{O}_8$ at $T \lesssim 200\text{K}$, as we see from Fig. 1. However, we note that the aspect ratio $\gamma \approx 0.14$, giving the best fit of resistivity curves, coincides within the accuracy of our model with the ratio of coherence lengths along and perpendicular to conducting layers. This may indicate that SC fluctuations, probably heterogeneous and located at the SC islands, may also be partially responsible for the resistivity drop and nonzero $\phi(T)$ at $T \sim 200\text{K}$.

The alternative interpretation of the resistivity decrease in $\text{YBa}_2\text{Cu}_4\text{O}_8$ in the interval $T_c < T < T^*$ is based on the crossover between coherent metallic at low T and incoherent at high T interlayer transport.¹⁷ The idea of such a crossover was developed to explain the nonmonotonic temperature dependence of interlayer conductivity observed in various layered conductors, including graphite compounds,⁵⁶ TaS_2 ,⁵⁷ Sr_2RuO_4 ,⁵⁸ organic metals⁵⁹ etc. The most puzzling in this nonmetallic be-

havior was that the nonmonotonic temperature dependence of resistivity with a maximum at $\sim 100K$ was observed only along the interlayer direction, while the in-plane conductivity shows metallic behavior. First, this crossover from coherent to incoherent interlayer transport was believed to happen when the electron intralayer mean scattering time τ becomes greater than the interlayer hopping time $\tau_z = \hbar/t_z$, so that electrons scatter many times before tunneling to the adjacent layer. The limit $\tau/\tau_z \ll 1$ received the special term “weakly incoherent”, but even in magnetoresistance no considerable changes of behavior have been found at $\tau/\tau_z \ll 1$.⁶⁰ Later it was realized that even at $\tau/\tau_z \ll 1$ the coherent interlayer transport survives, and one needs to include the phonon-assisted interlayer tunneling or/and resonance impurities between the conducting layers into the theoretical model to explain such behavior.^{61–63} In any case, the resistivity decrease at $T_c < T < T^*$ in $YBa_2Cu_4O_8$ is, probably, mainly due to the heterogeneous SC onset discussed above rather than due to this coherence-incoherence crossover, because the analyzed experimental data¹⁷ on the temperature dependence of resistivity in $YBa_2Cu_4O_8$ do not have the resistance maximum, typical for this coherence-incoherence crossover. Moreover, these data corresponds to the samples with higher resistance at room temperature, suggesting their strong spatial inhomogeneity. Of course, both these effects, namely, SC inclusions and the incoherent channels of conductivity may be present and contribute in parallel, leading to the observed decrease of resistivity in $YBa_2Cu_4O_8$ below 250K.

The proposed model and analytical results are rather general and can be used for the analysis of experimental data in other strongly anisotropic compounds. Let us briefly summarize the main steps of the comparison of this model with experimental data. First, one chooses a compound where, presumably, superconductivity appears in the form of isolated islands. This is very helpful, but not necessary, if there are STM or other measurements, supporting this heterogeneous SC onset and giving the typical size of SC inclusions. Then one extracts from experimental resistivity data the excess conductivity as a function of temperature along three main axes due to superconducting inclusions. This can be done more easily if there are also experimental data on conductivity in magnetic field or under other conditions, suppressing superconductivity. If the resistivity data without superconducting inclusions are not available, the excess conductivity can be approximately extracted using the extrapolation from higher temperature, where superconductivity is suppressed. These data on excess conductivity along main axes are fitted by the formulas derived above, which gives the temperature dependence of the volume fraction $\phi(T)$ of superconducting inclusions and their aspect ratios γ and β . If, in addition to transport measurements, the diamagnetic response due to superconducting inclusions is measured, it can be used for independent measure of $\phi(T)$. The comparison of $\phi(T)$

from resistivity and susceptibility measurements is helpful to check the consistency and applicability of the proposed model to studied material. It can also be used to estimate the size of superconducting inclusions.

VI. CONCLUSIONS

In this paper we developed a classical model and derived analytical expressions, given by Eqs. (12)-(14) and (B1)-(B6), for conductivity in a heterogeneous fully anisotropic conductors with ellipsoid superconducting inclusions. This model and the analytical results obtained are useful and convenient to analyze experimental data on the temperature dependence of conductivity anisotropy in various anisotropic superconductors, where superconductivity onset happens inhomogeneously in the form of isolated superconducting islands. We illustrate this by analyzing the experimental data on the temperature dependence of resistivity along three main axes above the transition temperature T_c in the high-temperature superconductor $YBa_2Cu_4O_8$ and in the organic superconductor β -(BEDT-TTF)₂I₃. In β -(BEDT-TTF)₂I₃ we compared the temperature dependence of the superconductivity fraction extracted from resistivity and diamagnetic response data, which allows estimating the size of superconducting inclusions as $d \sim 1\mu m$. We described the comparison between our theory and the experimental data in detail, to make this procedure clear for applications to other anisotropic superconductors. In spite of its simplicity, the proposed classical model of anisotropic heterogeneous superconductor gives a reasonable qualitative and often quantitative description of the temperature dependence of resistivity and of its anisotropy above the transition temperature in the compounds with inhomogeneous superconductivity onset in the form of isolated superconducting islands.

Acknowledgments

We thank Yaroslav Gerasimenko and Konstantin Tikhonov for useful discussions. The paper was partially supported by the Ministry of Education and Science of the Russian Federation in the framework of Increase Competitiveness Program of NUST MISiS and by “Basis” Foundation. Sec. V was supported by the Russian Science Foundation (Grant No. 16-42-01100). P.G. acknowledges the program 0033-2018-0001 “Condensed Matter Physics” by the FASO of Russia. P.K. acknowledges the support of Arconic Foundation.

Appendix A: Conductivity anisotropy in the standard theory of superconducting fluctuations

The model in Refs. [19,20] predicts that if superconductivity in an anisotropic conductors appears in

the form of isolated superconducting islands, it reduces electric resistivity anisotropically with the maximal effect along the least conducting axis. This prediction is supported by the experimental data in various compounds.^{17–23} These results cannot be explained by the standard theory²⁴ of superconducting fluctuations in homogeneous superconductors, as was argued in Ref. [20]. In this appendix section we briefly repeat these arguments²⁰ for completeness and discuss possible extensions of the homogeneous theory of superconducting fluctuations.

According to Chapter 3 of Ref. [24] within the time-dependent Ginzburg-Landau equations (i.e., near T_c), the excess conductivity due to fluctuations in layered quasi-2D superconductors in the absence of a magnetic field is given by the expressions

$$\Delta\sigma_{xx}(\epsilon, h=0, \omega=0) = \frac{e^2}{16s} \frac{1}{\sqrt{\epsilon(\epsilon+r)}}, \quad (\text{A1})$$

$$\Delta\sigma_{zz}(\epsilon, h=0, \omega=0) = \frac{e^2 s}{32\xi_{xy}^2} \left(\frac{\epsilon+r/2}{\sqrt{\epsilon(\epsilon+r)}} - 1 \right), \quad (\text{A2})$$

where s is interlayer distance, $r = 4\xi_z^2(0)/s^2$, ξ_{xy} and ξ_z denote the superconducting coherence length in the conducting layers and across them, respectively; and $\epsilon \equiv \ln(T/T_c) \approx (T - T_c)/T_c \ll 1$. At $\epsilon \ll r$ Eq. (A2) gives

$$\Delta\sigma_{zz} \approx \frac{e^2 s}{16\xi_{xy}^2} \frac{\xi_z^2(0)/s^2}{\sqrt{\epsilon(\epsilon+r)}} = \Delta\sigma_{xx} \frac{\xi_z^2(0)}{\xi_{xy}^2}, \quad (\text{A3})$$

and at $r \ll \epsilon$ from Eq. (A2) we have

$$\Delta\sigma_{zz} = \frac{e^2 s}{32\xi_{xy}^2} \frac{r^2}{8\epsilon^2} \ll \Delta\sigma_{xx} \frac{s^2}{\xi_{xy}^2}. \quad (\text{A4})$$

In both cases, the excess conductivity across conducting layers $\Delta\sigma_{zz}$ is much lower (namely, by the parameters $\xi_z^2/\xi_{xy}^2 \ll 1$ or $s^2/\xi_{xy}^2 \ll 1$) than the excess conductivity along the layers $\Delta\sigma_{xx}$. This small parameter $\xi_z^2/\xi_{xy}^2 \sim v_z^2/v_x^2 \sim \sigma_{zz}/\sigma_{xx}$. Hence, within the Ginzburg-Landau theory, the relative increase of conductivity due to superconducting fluctuations is isotropic, which cannot explain the observed^{17–23} temperature dependence of conductivity anisotropy above T_c .

A stricter microscopic theory of the fluctuation contribution to the conductivity (see Chapter 7 in [24] and references therein) is applicable far away from T_c and includes not only the Aslamazov-Larkin correction given by Eqs. (A1)–(A4) but also the Maki-Thompson correction and the correction due to the renormalization of electron density of states. However, this stricter theory predicts⁶⁴ an increase in the transverse resistance (not conductivity!) above T_c , observed⁶⁵ in some cuprates as a resistance peak just above T_c . Thus, the much stronger excess conductivity across the conducting layers cannot be explained within the existing theory²⁴ of fluctuation conductivity in spatially homogeneous superconductors.

A possible extension of the existing homogeneous theory²⁴ of SC fluctuations to a spatially inhomogeneous superconductors, where SC fluctuations appear only in some special spots, may be useful to explain the observed anisotropic correction to resistivity far above T_c , where the SC volume fraction according to our model is very small. Such spots of highly probable SC fluctuations somewhat resemble the spots of higher conductivity in our model of SC islands, but instead of steady SC islands with zero resistance one takes islands with reduced resistance due to SC fluctuations. The frequency dependence of conductivity in such a heterogeneous theory of SC fluctuations, probably, differ considerably from that in our model. Such a model of heterogeneous SC fluctuations, being beyond the scope of this paper, may be relevant and useful for superconductors with nonuniform doping concentration, with nonuniform charge- or spin-density wave structure, or with other types of heterogeneity.

Appendix B: Elliptic integrals

In this appendix we calculate integrals (8) and find exact expressions for coefficients A_1, A_2, A_3 as well as their asymptotic behaviors for different cases.

Let $a_1 < a_2 < a_3$. Denote $\nu = \arcsin \sqrt{a_3^2 - a_1^2}/a_3$ – angular eccentricity; $q = \sqrt{(a_3^2 - a_2^2)/(a_3^2 - a_1^2)}$; $q' \equiv \sqrt{1 - q^2} = \sqrt{(a_2^2 - a_1^2)/(a_3^2 - a_1^2)}$. Using the table elliptic integrals (integrals 6, 12, 18 from Sec. 3.133 of Ref. [66]) we obtain:

$$\begin{aligned} A_1 &= \frac{a_1 a_2 a_3}{2} \int_0^\infty \frac{dt}{(t + a_1^2) \sqrt{(t + a_1^2)(t + a_2^2)(t + a_3^2)}} = \\ &= \frac{a_1 a_2 a_3}{2} \left(\frac{2}{(a_1^2 - a_2^2) \sqrt{a_3^2 - a_1^2}} E(\nu, q) + \frac{2}{a_2^2 - a_1^2} \frac{a_2}{a_1 a_3} \right). \end{aligned} \quad (\text{B1})$$

$$\begin{aligned} A_2 &= \frac{a_1 a_2 a_3}{2} \int_0^\infty \frac{dt}{(t + a_2^2) \sqrt{(t + a_1^2)(t + a_2^2)(t + a_3^2)}} = \\ &= \frac{a_1 a_2 a_3}{2} \left(\frac{2\sqrt{a_3^2 - a_1^2}}{(a_2^2 - a_1^2)(a_3^2 - a_2^2)} E(\nu, q) - \right. \\ &\quad \left. \frac{2}{(a_3^2 - a_2^2) \sqrt{a_3^2 - a_1^2}} F(\nu, q) - \frac{2}{a_2^2 - a_1^2} \frac{a_1}{a_2 a_3} \right). \end{aligned} \quad (\text{B2})$$

$$\begin{aligned} A_3 &= \frac{a_1 a_2 a_3}{2} \int_0^\infty \frac{dt}{(t + a_3^2) \sqrt{(t + a_1^2)(t + a_2^2)(t + a_3^2)}} = \\ &= \frac{a_1 a_2 a_3}{2} \left(\frac{2}{(a_3^2 - a_2^2) \sqrt{a_3^2 - a_1^2}} (F(\nu, q) - E(\nu, q)) \right). \end{aligned} \quad (\text{B3})$$

Here $F(\nu, q)$ and $E(\nu, q)$ are incomplete elliptic integrals of the first and the second kind respectively with amplitude ν and the elliptic modulus q [66]. It can be easily checked that indeed $A_1 + A_2 + A_3 = 1$.

Let us simplify formulas (B1)-(B3) for two limiting cases: (i) $a_3 \gg a_1, a_2$; (ii) $a_2 - a_1 \ll a_3$.

(i) $a_3 \gg a_1, a_2$. In this case $\nu \rightarrow \pi/2$ and $q \rightarrow 1$. Using the double asymptotic expansions for $F(\nu, q)$ and $E(\nu, q)$ [67], we find

$$A_1 \approx \frac{a_2}{a_1 + a_2} - \frac{a_1 a_2}{2a_3^2} \ln \frac{4a_3/e}{a_1 + a_2}, \quad (\text{B4})$$

$$A_2 \approx \frac{a_1}{a_1 + a_2} - \frac{a_1 a_2}{2a_3^2} \ln \frac{4a_3/e}{a_1 + a_2}, \quad (\text{B5})$$

$$A_3 \approx \frac{a_1 a_2}{a_3^2} \ln \frac{4a_3/e}{a_1 + a_2}. \quad (\text{B6})$$

Substituting here a_i from formula (6), we get

$$A_1 \approx \frac{\beta}{\sqrt{\mu} + \beta}, \quad (\text{B7})$$

$$A_2 \approx \frac{\sqrt{\mu}}{\sqrt{\mu} + \beta}, \quad (\text{B8})$$

$$A_3 \approx \frac{\beta\eta}{\gamma^2\sqrt{\mu}} \ln \frac{4\gamma}{e\sqrt{\eta}(1 + \beta/\sqrt{\mu})}. \quad (\text{B9})$$

(ii) The case $a_2 - a_1 \ll a_3$ (i.e. $a_2 - a_1 \rightarrow 0$). In this case $q \rightarrow 1$ and we use $E(\nu, q) = E(\nu, \sqrt{1 - q^2}) \approx \sin \nu + 1/2(\ln((1 + \sin \nu)/\cos \nu) - \sin \nu)q'^2$; $F(\nu, q) \approx F(\nu, 1) = \ln((1 + \sin \nu)/\cos \nu)$ and obtain

$$A_1 \approx A_2 \approx \frac{1}{2} - \frac{a_1^2 a_3}{2(a_3^2 - a_1^2)^{3/2}} \ln \frac{a_3 + \sqrt{a_3^2 - a_1^2}}{a_1} + \frac{a_1^2}{2(a_3^2 - a_1^2)}. \quad (\text{B10})$$

$$A_3 \approx \frac{a_1^2 a_3}{(a_3^2 - a_1^2)^{3/2}} \ln \frac{a_3 + \sqrt{a_3^2 - a_1^2}}{a_1} - \frac{a_1^2}{a_3^2 - a_1^2} \quad (\text{B11})$$

For $a_1 = a_2$ formulas (B10)-(B11) become exact. In the double limit $(a_2 - a_1) \rightarrow 0$ and $a_3/a_1 \rightarrow \infty$ we get $A_3 \sim (a_1^2/a_3^2) \ln(2a_3/ea_1)$, which coincides with (B6) when $a_1 = a_2$. Recalling that $a_1/a_3 = \sqrt{\eta_*} \equiv \sqrt{\eta}/\gamma$ we can recast (B11) into

$$A_3 \approx \frac{\eta_*}{(1 - \eta_*)^{3/2}} \ln \frac{1 + \sqrt{1 - \eta_*}}{\sqrt{\eta_*}} - \frac{\eta_*}{1 - \eta_*}, \quad (\text{B12})$$

which after algebraic manipulations can be transformed into the form of Eq. (17.30) of Ref. [26] or Eq. (5) of Ref. [19]. For $\eta_* \rightarrow 0$ the formula (B12) simplifies to $A_3 \sim \eta_* \ln(1/\eta_*)/2$, which is consistent with Eq. (6) of [19].

* Electronic address: karpov.petr@gmail.com

† Electronic address: grigorev@itp.ac.ru

¹ B. Keimer, S. A. Kivelson, M. R. Norman, S. Uchida, & J. Zaanen, *Nature* **518**, 179 (2015).

² Qimiao Si, Rong Yu, & Elihu Abrahams, *Nature Reviews Materials* **1**, 16017 (2016).

³ Yu.V. Pustovit and A.A. Kordyuk, *Low Temperature Physics* **42**, 995 (2016).

⁴ V.Z. Kresin, Yu.N. Ovchinnikov and S.A. Wolf, *Physics Reports* **431**, 231 (2006).

⁵ K.M. Lang, V. Madhavan, J.E. Hoffman, E.W. Hudson, H. Eisaki, S. Uchida & J.C. Davis, *Nature* **415**, 412 (2002).

⁶ W.D. Wise, Kamallesh Chatterjee, M.C. Boyer, Takeshi Kondo, T. Takeuchi, H. Ikuta, Zhijun Xu, Jinsheng Wen, G.D. Gu, Yayu Wang & E.W. Hudson, *Nature Physics* **5**, 213 (2009).

⁷ Anand Kamlapure, Tanmay Das, Somesh Chandra Ganguli, Jayesh B. Parmar, Somnath Bhattacharyya & Pratap Raychaudhuri, *Scientific Reports* **3**, 2979 (2013).

⁸ Krzysztof Gofryk, Minghu Pan, Claudia Cantoni, Bayrammurad Saparov, Jonathan E. Mitchell, and Athena S. Sefat, *Phys. Rev. Lett.* **112**, 047005 (2014).

⁹ Anton Fente, Alexandre Correa-Orellana, Anna E. Bohmer, Andreas Kreyssig, S. Ran, Sergey L. Bud'ko, Paul

C. Canfield, Federico J. Mompean, Mar Garcia-Hernandez, Carmen Munuera, Isabel Guillaumon, and Hermann Suderow, *Phys. Rev. B* **97**, 014505 (2018).

¹⁰ Yu.G. Naidyuk, G. Fuchs, D.A. Chareev, and A.N. Vasiliev, *Phys. Rev. B* **93**, 144515 (2016).

¹¹ Lu Li, Yayu Wang, Seiki Komiya, Shimpei Ono, Yoichi Ando, G. D. Gu, and N. P. Ong, *Phys. Rev. B* **81**, 054510 (2010).

¹² Lucia Cabo, Felix Soto, Mauricio Ruibal, Jesus Mosqueira, and Felix Vidal, *Phys. Rev. B* **73**, 184520 (2006).

¹³ Ienari Iguchi, Tetsuji Yamaguchi & Akira Sugimoto, *Nature* **412**, 420 (2001).

¹⁴ P. Carretta, A. Lascialfari, A. Rigamonti, A. Rosso, and A. Varlamov, *Phys. Rev. B* **61**, 12420 (2000).

¹⁵ Akira Sugimoto, Ienari Iguchi, Takashi Miyake and Hisashi Sato, *Japanese Journal of Applied Physics* **41**, L497 (2002).

¹⁶ C. Bergemann, A.W. Tyler, A.P. Mackenzie, J.R. Cooper, S.R. Julian, and D.E. Farrell, *Phys. Rev. B* **57**, 14387 (1998).

¹⁷ N. E. Hussey, K. Nozawa, H. Takagi, S. Adachi and K. Tanabe, *Phys. Rev. B* **56**, R11423(R) (1997).

¹⁸ M.A. Tanatar, N. Ni, A. Thaler, S.L. Bud'ko, P.C. Canfield, and R. Prozorov, *Phys. Rev. B* **82**, 134528 (2010).

- ¹⁹ A. A. Sinchenko, P. D. Grigoriev, A. P. Orlov, A. V. Frolov, A. Shakin, D. A. Chareev, O. S. Volkova, and A. N. Vasiliev, Phys. Rev. B **95**, 165120 (2017).
- ²⁰ P.D. Grigoriev, A.A. Sinchenko, K.K. Kesharpur, A. Shakin, T.I. Mogilyuk, A.P. Orlov, A.V. Frolov, D.S. Lyubshin, D.A. Chareev, O.S. Volkova, A.N. Vasiliev, JETP Lett. **105**, 786 (2017).
- ²¹ L. I. Buravov, M. V. Kartsovnik, P. A. Kononovich, V. N. Laukhin, S. I. Pesotskii, and I. F. Shchegolev, Sov. Phys. JETP **64**, 1306 (1986) [Zh. Eksp. Teor. Fiz. **91**, 2198 (1986)].
- ²² N. Kang, B. Salameh, P. Auban-Senzier, D. Jerome, C. R. Pasquier, and S. Brazovskii, Phys. Rev. B **81**, 100509(R)(2010).
- ²³ Ya. A. Gerasimenko, S. V. Sanduleanu, V. A. Prudkoglyad, A. V. Kornilov, J. Yamada, J. S. Qualls, and V. M. Pudalov, Phys. Rev. B **89**, 054518 (2014).
- ²⁴ A. Larkin and A. Varlamov, *Theory of Fluctuations in Superconductors* (Oxford Science, Oxford, 2007; Dobrosvet, Moscow, 2007).
- ²⁵ M. Tinkham, *Introduction To Superconductivity* (2d ed., McGraw-Hill, Inc., New York, 1996)
- ²⁶ S. Torquato, *Random Heterogeneous Materials*, Springer, 2001.
- ²⁷ *The Physics of Organic Superconductors and Conductors*, ed. by A. G. Lebed (Springer Series in Materials Science, V. 110; Springer Verlag Berlin Heidelberg 2008).
- ²⁸ T. Ishiguro, K. Yamaji and G. Saito, *Organic Superconductors*, 2nd Edition, Springer-Verlag, Berlin, 1998.
- ²⁹ D. Andres, M. V. Kartsovnik, W. Biberacher, K. Neumaier, E. Schuberth, and H. Muller, Phys. Rev. B **72**, 174513 (2005).
- ³⁰ L.P. Gor'kov, P.D. Grigoriev, Phys. Rev. B **75**, 020507(R) (2007).
- ³¹ P.D. Grigoriev, Phys. Rev. B **77**, 224508 (2008).
- ³² P.D. Grigoriev, Physica B **404**, 513 (2009).
- ³³ P.D. Grigoriev, S.S. Kostenko, Physica B **460**, 26 (2015).
- ³⁴ A.Narayanan, A. Kiswandi, D. Graf, J. Brooks, & P. Chaikin, Phys. Rev. Lett. **112**, 146402 (2014).
- ³⁵ L. Buravov, N. Kushch, V. Merzhanov, M. Osherov, A. Khomenko, E. Yagubskii, J. Phys. I France **2**, 1257 (1992).
- ³⁶ Satoshi Tsuchiya, Jun-ichi Yamada, Satoshi Tanda, Koichi Ichimura, Taichi Terashima, Nobuyuki Kurita, Kota Kodama, and Shinya Uji Phys. Rev. B **85**, 220506(R) (2012).
- ³⁷ Yoichi Ando, Kouji Segawa, Seiki Komiyama, and A.N. Lavrov, Phys. Rev. Lett. **88**, 137005 (2002).
- ³⁸ Rafael M. Fernandes, Elihu Abrahams, and Jorg Schmalian, Phys. Rev. Lett. **107**, 217002 (2011).
- ³⁹ V. F. Kaminskii, T. G. Prokhorova, R. P. Shibaeva, E.B. Yagubskii, Pisma Zh. Eksp. Teor. Fiz **39**, 15 (1983) [JETP Lett. **39**, 17 (1983)].
- ⁴⁰ E. B. Yagubskii, I. F. Shchegolev, V. N. Laukhin, Kononovich P. A., Kartsovnik M. V., Zvarykina A. V., Buravov L. I., Pisma Zh. Eksp. Teor. Fiz, **39** 12 (1984) [JETP Lett. **39**, 12 (1984)].
- ⁴¹ Data for resistivity for all three axes are available only for filled and blank circle samples. Of these two, the blank-circle data have been taken because of its smaller temperature step and less irregularities in the data.
- ⁴² V.A. Merzhanov, E.E. Kostyuchenko, V. N. Laukhin, R. M. Lobkovskaya, M. K. Makova, R. P. Shibaeva, I. F. Shchegolev, and E. B. Yagubskii, Pisma Zh. Eksp. Teor. Fiz **41**, 146 (1985) [JETP Lett. **41**, 179 (1985)].
- ⁴³ J.A. Cape, and J.M. Zimmerman, Phys. Rev. **153**, 416 (1967).
- ⁴⁴ L.D. Landau and E.M. Lifshits, *Electrodynamics of continuous media*, Pergamon (1984).
- ⁴⁵ J. Osborn, Phys. Rev. **67**, 351 (1945).
- ⁴⁶ Since the upper critical field for β -(BEDT-TTF)₂I₃ along the c -axis is about one order less than 2.8kOe, we assume that magnetic field in Ref. [42] is applied along the conducting plane. If it was applied not along b but along a -axis, the corresponding demagnetization factor would be $n \approx 0.1$ instead of the used value $n \approx 0.05$, and the factor $\sqrt{1-n}$ entering the estimate of SC island radius R in Eq. (18) would be almost the same.
- ⁴⁷ S.V. Dordevic, D.N. Basov and C.C. Homes, Scientific Reports **3**, 1713 (2013).
- ⁴⁸ L.N. Bulaevskii, V.B. Ginodman, A.V. Gudenko, Pisma Zh. Eksp. Teor. Fiz **45**, 355 (1987) [JETP Lett. **45**, 451 (1987)].
- ⁴⁹ E. A. Shapoval, JETP Lett. **69**, 577 (1999).
- ⁵⁰ M. Sahimi, *Heterogeneous Materials I - Linear Transport and Optical Properties* (Springer-Verlag, New York, Inc., 2003).
- ⁵¹ I. S. Beloborodov, A. V. Lopatin, V. M. Vinokur, and K. B. Efetov, Rev. Mod. Phys. **79**, 469 (2007).
- ⁵² I. Sternfeld, V. Shelukhin, A. Tsukernik, M. Karpovskii, A. Gerber, and A. Palevski, Phys. Rev. B **71**, 064515 (2005).
- ⁵³ P. Pureur, R. Menegotto Costa, P. Rodrigues, Jr., J. Schaf, and J. V. Kunzler, Phys. Rev. B **47**, 11420 (1993).
- ⁵⁴ V. Kresin, Yu.Ovchinnikov, and S. Wolf, Appl. Phys. Lett. **83**, 722 (2003).
- ⁵⁵ L. Ponta, A. Carbone, M. Gilli, and P. Mazzetti, Phys. Rev. B **79**, 134513 (2009).
- ⁵⁶ See N. B. Brandt, S. M. Chudinov, and Ya.G. Ponomarev, Semimetals: I. Graphite and its Compounds (North-Holland, Amsterdam, 1988) and references therein.
- ⁵⁷ W. J. Wattamaniuk, J. P. Tidman, and R. F. Frindt, Phys. Rev. Lett. **35**, 62 (1975).
- ⁵⁸ A.W. Tyler, A.P. Mackenzie, S. NishiZaki, and Y. Maeno, Phys. Rev. B **58**, R10107 (1998).
- ⁵⁹ J.G. Analytis, A. Ardavan, S.J. Blundell, R.L. Owen, E.F. Garman, C. Jeynes, and B.J. Powell, Phys. Rev. Lett. **96**, 177002 (2006).
- ⁶⁰ P. Moses and R.H. McKenzie, Phys. Rev. B **60**, 7998 (1999).
- ⁶¹ A. A. Abrikosov, Physica C **317-318**, 154 (1999).
- ⁶² D.B. Gutman and D.L. Maslov, Phys. Rev. Lett. **99**, 196602 (2007).
- ⁶³ M. V. Kartsovnik, P. D. Grigoriev, W. Biberacher, and N. D. Kushch, Phys. Rev. B **79**, 165120 (2009).
- ⁶⁴ L. B. Ioffe, A. I. Larkin, A. A. Varlamov, and L. Yu, Phys. Rev. B **47**, 8936 (1993).
- ⁶⁵ G. Balestrino, E. Milani, C. Aruta, and A. A. Varlamov, Phys. Rev. B **54**, 3628 (1996).
- ⁶⁶ Table of Integrals, Series, and Products. I.S. Gradshteyn and I.M. Ryzhik. 7-th edition (2007).
- ⁶⁷ E.L. Kaplan, J. Math. Physics **27**, 11 (1948).